Journal of Alloys and Compounds 503 (2010) 103–110

Contents lists available at ScienceDirect

Journal of Alloys and Compounds

journal homepage: www.elsevier.com/locate/jallcom

Preparation and photocatalytic property of mesoporous ZnO/SnO_2 composite nanofibers

Ruilai Liu[a,d], Yingxing Huang[c], Aihua Xiao[a], Haiqing Liu[a,b,*]

[a] College of Chemistry and Materials Science, Fujian Normal University, Fuzhou 350007, China
[b] Key Laboratory of Polymer Materials of Fujian Province, Fuzhou 350007, China
[c] Key Laboratory of Photocatalytic of Fujian Province, Fuzhou University, Fuzhou 350006, China
[d] Department of Chemistry and Environment Engineering, Wuyi University, Wuyishan 354300, China

ARTICLE INFO

Article history:
Received 30 December 2009
Received in revised form 25 April 2010
Accepted 28 April 2010
Available online 5 May 2010

Keywords:
ZnO
Nanofibers
Electrospinning
Photocatalyst
Mesopores

ABSTRACT

In this paper, we prepared mesoporous ZnO/SnO_2 composite nanofibers via the electrospinning technique using zinc acetate ($Zn(OAc)_2$) and stannic chloride pentahydrate ($SnCl_4{\cdot}5H_2O$) as precursors, cellulose acetate (CA) as the fiber template, and N,N-dimethylformamide (DMF)/acetone (1:1, v/v) as the co-solvent. The structure and morphology of composite nanofibers were characterized by scanning electron microscopy (SEM), transmission electron microscopy (TEM), X-ray diffraction (XRD), UV–vis diffuse reflectance spectroscopy (DRS) and nitrogen adsorption–desorption isotherm analysis. TEM images showed that the mesoporous ZnO/SnO_2 composite nanofibers were composed of grain-like nanoparticles. The nanoparticles size increased with the increasing of the calcination temperature from 500 to 900 °C. Moreover, the crystal phases, grain sizes, and band gap energy of the mesoporous ZnO/SnO_2 composite nanofibers were influenced by the molar ratio of Zn:Sn and the calcination temperatures. The photocatalytic activity of the mesoporous ZnO/SnO_2 composite nanofibers toward the decomposition of Rhodamine B (RhB) was investigated. It was found that the photocatalytic activity of the mesoporous ZnO/SnO_2 composite nanofibers was dependant on their surface areas, light utilization efficiency, and the separation of photogenerated electron/hole pairs. The maximum photocatalytic activity was shown for composite nanofibers with the molar ratio of Zn:Sn = 2:1 and calcination at 500 °C for 5 h, more or less Zn:Sn ratios lowered the photocatalytic efficiency. A mechanism of the charge separation and photocatalytic reaction for the mesoporous ZnO/SnO_2 composite nanofibers was also presented.

1. Introduction

Environmental pollutions caused by detergents, dyes, and pesticides in water have provided the impetus for sustained fundamental and applied research interest in the area of environmental remediation [1,2]. Photocatalytic degradation of organic pollutants by nanostructured semiconductors offers great potentials for the complete elimination of toxic chemicals. The wide-band gap semiconductor metal oxides such as TiO_2 and ZnO have been the subject of great research interest due to their size-tunable physicochemical properties, high activities, and non-selective degradability toward various organic pollutants under UV irradiation [3–5].

Most of the current semiconductor photocatalysts are in the form of particles. However, the particles readily agglomerate during aging, and they may repollute the treated water due to difficult recovery. Such difficulty becomes more serious for the recovery of particles with size down to nanometer [6,7]. In order to overcome this shortcoming, semiconductor photocatalysts were immobilized onto inorganic porous carriers such as silica, zeolite, stainless steel, and organic polymers [8–10]. The immobilization prevents particles from agglomeration and makes them to be reclaimed easily from reaction mixtures at high yields [11,12]. However, immobilized photocatalysts usually suffer a significant loss in surface areas, and therefore lower their photocatalytic efficiency [6]. Moreover, the immobilization process is too complicated to show any practical privileges [13]. Therefore, the development of new types of nanostructured photocatalyst with efficient electron/hole utilization, high surface areas, favorable recycling characteristics and simple preparation is very important for practical applications.

Due to the very large specific surface areas and length to diameter ratio of a fiber, photocatalysts in the fiber morphology is superior to the particle form as far as the recycling and aggregation are concerned [14,15]. Amongst many methods such as hydrothermal and vapor-phase transport used for the preparation of nanofibers, electrospinning is the only method able to yield

* Corresponding author at: College of Chemistry and Materials Science, Fujian Normal University, Fuzhou 350007, China.
Tel.: +86 591 83597537; fax: +86 591 83465225.
E-mail address: haiqing.liu@gmail.com (H. Liu).

0925-8388/$ – see front matter © 2010 Elsevier B.V. All rights reserved.
doi:10.1016/j.jallcom.2010.04.211

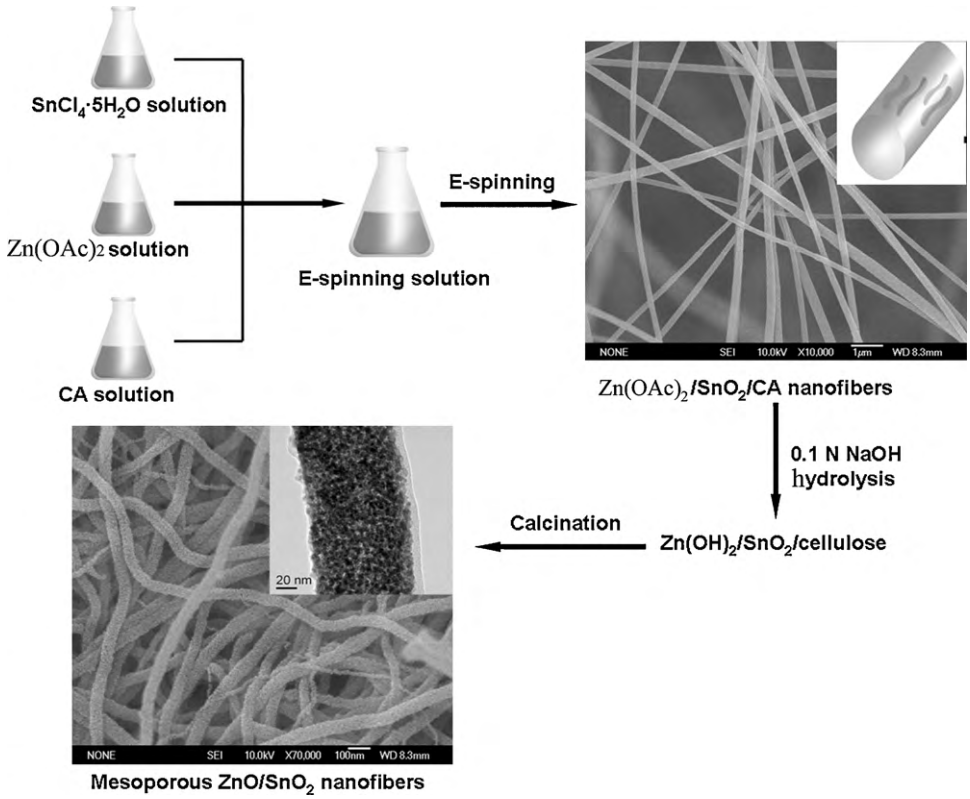

Fig. 1. The preparation procedure of mesoporous ZnO/SnO_2 composite nanofiber through electrospinning

abundant quantities of continuous nanofibers with diameter down to tens of nanometers and length up to several centimeters [16–19].

Several important semiconductor metal oxides such as TiO_2 [20], ZnO [21], NiO [22], ZnS [23], and Bi_2O_3 [24] nanofibers were fabricated by electrospinning. They not only show photocatalytic efficiency toward the degradation of methylene blue, Rhodamine B and phenol, but also good reclaiming ability. In order to enhance the photocatalytic activity of single component nanofibers, composite nanofibers with two components such as TiO_2/ZnO [25], TiO_2/SnO_2 [26], TiO_2/CdO [27] and TiO_2/SiO_2 [28] composite nanofibers were also prepared.

Although SnO_2 itself has little photocatalytic efficiency, it has been reported that the incorporation of low content of SnO_2 in TiO_2 nanofibers greatly enhances the photocatalytic activity of TiO_2 [29,30]. Additionally, electrospun SnO_2 [31] and ZnO/SnO_2 [32,33] composite nanofibers were applied as highly efficient gas sensors for the detection of ethanol, toluene, O_2 and NO_2. However, the photocatalytic activity of ZnO/SnO_2 composite nanofibers has not been studied so far.

The objective of this work is to enhance the photocatalytic activity of ZnO nanofibers by coupling with SnO_2. SnO_2 nanofibers have often been prepared by using organotin as the precursor, ethanol/water soluble polymer polyvinyl pyrrolidine (PVP) as the fiber template. It's well known that the organtin is toxic and has a bad odor, so it is better to use inorganic salt stannic chloride pentahydrate ($SnCl_4$) as the precursor. Cellulose acetate (CA) is easily soluble in many common solvents, and it is a good fiber-forming polymer through electrospinning [21]. In this paper, we prepare mesoporous ZnO/SnO_2 composite nanofibers through electrospinning $Zn(OAc)_2$ and $SnCl_4{\cdot}5H_2O$ as precursors and cellulose acetate (CA) as the fiber template in mixed solvent N,N-dimethylformamide (DMF)/acetone (1:1, v/v). Then the mesoporous ZnO/SnO_2 composite nanofibers are prepared by calcination of $Zn(OH)_2/SnO_2$/cellulose composite nanofibers, which is obtained from the hydrolysis of $Zn(OAc)_2/SnO_2$/CA composite nanofibers in a base solution. Their morphology, crystal structure, and light absorption behavior are characterized by SEM, TEM, XRD, DRS and N_2 adsorption and desorption isotherm. Their photocatalytic efficiency is studied as a function of molar ratio of Zn:Sn, calcination temperature, and the crystal structure of the mesoporous ZnO/SnO_2 composite nanofibers. A photocatalytic mechanism is provided according to the data obtained in this study.

2. Experimental

2.1. Materials

Stannic chloride pentahydrate ($SnCl_4{\cdot}5H_2O$) and zinc acetate dihydrate ($Zn(OAc)_2{\cdot}2H_2O$) were purchased from Sinopharm Chemical Reagents Co., China. Zinc acetate was recrystallized before use. Cellulose acetate (CA) with degree of substitution (DS) of 2.45 and an M_w of 3.0×10^4 was obtained from Eastman, USA. All other chemicals were used as received.

2.2. Preparation of mesoporous ZnO/SnO_2 composite nanofibers

Transparent spinning solutions containing 2 wt.% $Zn(OAc)_2$ and $SnCl_4{\cdot}5H_2O$ were prepared by adding $Zn(OAc)_2$ and $SnCl_4{\cdot}5H_2O$ in the molar ratio of 3:1, 2:1 and 1:1 (labeled as Z_3S, Z_2S and ZS) into 18 wt.% CA in N,N-dimethylformamide (DMF)/acetone (1:1, v/v) solvent mixture, followed by magnetic stirring at ambient temperature. 5 mL of spinning solution was loaded into a plastic syringe equipped with a 18-gauge stainless steel needle. The feeding rate was 10 μL/min monitored by a syringe pump (TS2-60, Longer Precision Pump Co. Ltd., Baoding, China). An electrode was clamped on the needle and connected to a power supply (DW-P303-IAC, Tianjin Dongwen High Voltage Plant, China). A grounded counter electrode was connected to a collector aluminum foil, which was placed 12 cm away from the orifice. The electric field was kept at 10 kV. Such obtained composite nanofibrous mats on the grounded collector were kept in air for 12 h to allow the fully hydrolysis into $Zn(OAc)_2/SnO_2$/CA, and then dried in a vacuum oven at 90 °C for 5 h.

One part of $Zn(OAc)_2/SnO_2$/CA composite nanofibrous mats was calcined at 500 °C in air for 5 h. The other part of mats was hydrolyzed in 0.1 mol/L NaOH solution for 24 h at 25 °C to convert $Zn(OAc)_2/SnO_2$/CA composite nanofibers into $Zn(OH)_2/SnO_2$/cellulose composite nanofibers, then washed with distilled water completely. The hydrolyzed mats were vacuum dried at 50 °C for 5 h. Subsequently it was calcined at 500, 700 and 900 °C in air for 5 h, respectively. Accordingly, the

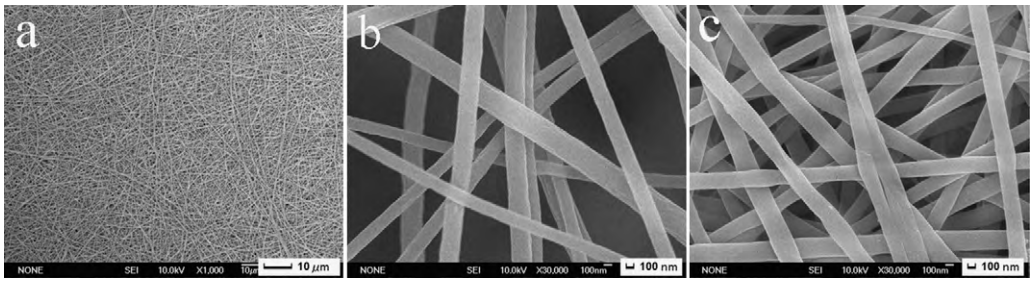

Fig. 2. Typical SEM images of (a) $Zn(OAc)_2/SnO_2$/CA composite nanofibers, (b) magnified image of (a), (c) $Zn(OH)_2/SnO_2$/cellulose composite nanofibers obtained form hydrolysis of (b) in aq. NaOH solution. a, b and c samples were from precursor solution containing $Zn(OAc)_2$ and $SnCl_4{\cdot}5H_2O$ in the molar ratio of 2:1.

resultant products were coded as Z_3S-5, Z_2S-7, ZS-9, Z_2S-5, Z_2S-7, Z_2S-9, ZS-5, ZS-7 and ZS-9 (the last number designates the calcination temperature). For comparison, pure ZnO (Z) and SnO_2 (S) nanofibers were prepared using the same procedure as mentioned above, and they were labeled as Z-5, Z-7, Z-9, S-5, S-7 and S-9. A schematic preparation procedure of mesoporous ZnO/SnO_2 composite nanofibers through electrospinning was illustrated in Fig. 1.

2.3. Characterization

X-ray diffraction (XRD) patterns were recorded on X'pert MPD Pro (Philips, Netherlands) with Cu Kα radiation (λ = 1.542 Å), over the 2θ range of 10–60°. An accelerating voltage of 40 kV, emission current of 30 mA and the scanning speed of 8° min^{-1} were used. The diameter and morphology of mesoporous ZnO/SnO_2 composite nanofibers were observed on SEM (JSM-7500LV, JEOL), and TEM (JEM2010, JEOL). Specimens were sputter coated with platinum before SEM observation. For TEM measurement, the fibers were dispersed ultrasonically in ethanol and were transferred onto Formvar-coated copper grids before observation. The porosity and specific surface areas were characterized by nitrogen adsorption–desorption isotherm analysis (Micromeritics ASAP2020 apparatus at 77 K). DRS spectra were recorded in air at 25 °C in the wavelength of 200–700 nm using a Hitachi U-3010 spectrophotometer with an integrating sphere. The pure powdered $BaSO_4$ was used as a reference.

2.4. Photocatalytic experiments

Photocatalytic experiments were conducted using ZnO/SnO_2 composite nanofibers to degrade Rhodamine B (RhB) in water solution. A photochemical reactor was set up according to our previous work [21,25]. The photocatalytic degradation reactions were carried out under atmospheric condition using a 500 W high pressure mercury lamp (Philips 365 nm) as the irradiation source at ambient temperature. The irradiation distance between the lamp and the sample was 10 cm. Five milligrams of nanofibers was added into a cylindrical glass vessel containing 10 g of 8 ppm RhB aqueous solution. The aqueous system was magnetically stirred in dark for 30 min to reach adsorption equilibrium of RhB on the nanofibers, and then exposed to UV light. At certain time interval, the degradation reaction was ceased and the solution was centrifuged. The RhB concentration in the supernatant was measured on a UV–vis spectrometer (Lambda850, PerkinElmer). Parallel degradation reactions under same conditions were conducted for varied time intervals.

3. Result and discussion

Fig. 2a shows the SEM images of $Zn(OAc)_2/SnO_2$/CA composite nanofibers. The fresh prepared composite fibers prepared from electrospinning were kept in air for 12 h to allow fully con-

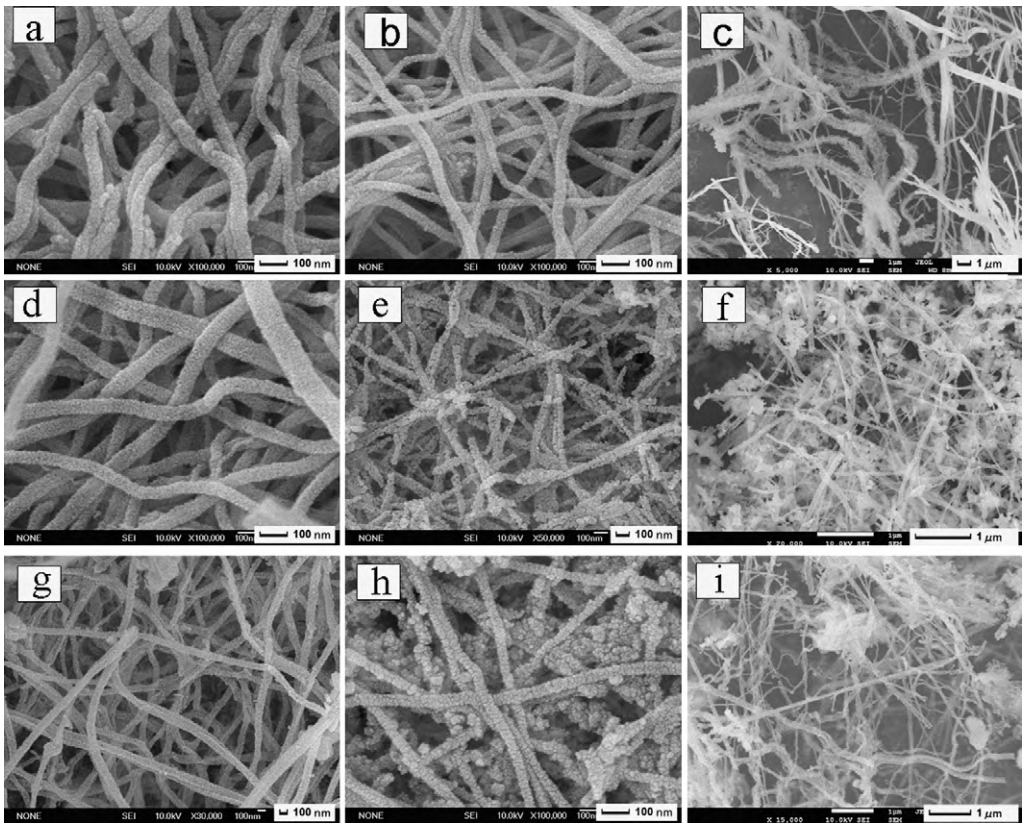

Fig. 3. SEM images of (a) Z_3S-5, (b) Z_2S-7, (c) ZS-9, (d) Z_2S-5, (e) Z_2S-7, (f) Z_2S-9, (g) ZS-5, (h) ZS-7, (i) ZS-9.

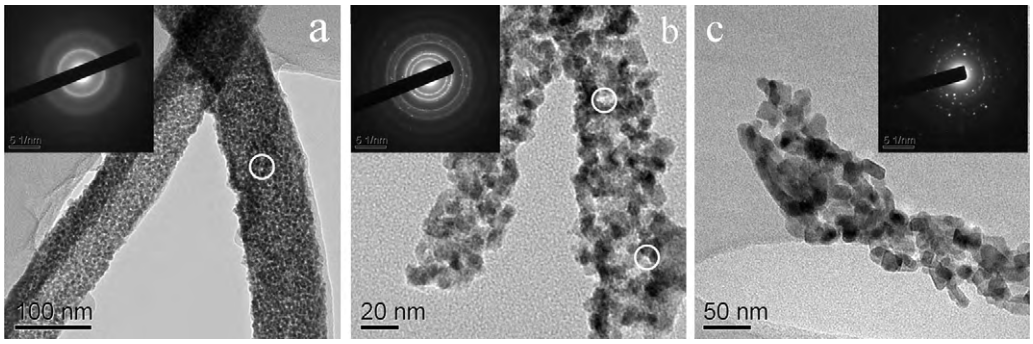

Fig. 4. TEM images of (a) Z_2S-5, (b) Z_2S-7, (c) Z_2S-9; inset is SAED image of corresponding mesoporous composite nanofibers.

version of $SnCl_4{\cdot}5H_2O$ component into SnO_2 due to the ready hydrolysis of $SnCl_4{\cdot}5H_2O$. The composite nanofibers were relatively smooth and round, and their average diameter was 180 ± 26 nm (Fig. 2b). Surprisingly, the calcination of $Zn(OAc)_2/SnO_2$/CA composite nanofibers at 500 °C in air generated sheet-particle instead of nanofibers (image not shown). This is due to that CA component is a thermoplastic with a T_m (melting temperature) and a T_d (decomposition temperature) at 230 and 340 °C [34], respectively. Therefore, the CA component in the $Zn(OAc)_2/SnO_2$/CA composite nanofibers melts upon heating, resulting in transformation from fiber to molten CA. With a further increasing of the oven temperature, CA is decomposed and ZnO/SnO_2 sheet-like particles are left behind. In order to obtain the ZnO/SnO_2 composite nanofibers instead of nanoparticles, the composite nanofibers were hydrolyzed in NaOH aq. solution to convert $Zn(OAc)_2/SnO_2$/CA composite nanofibers into $Zn(OH)_2/SnO_2$/cellulose composite nanofibers. The main objective is to convert CA into thermosetting cellulose. The two chemical reactions were described in the following Eqs (1) and (2):

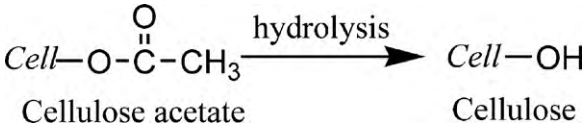

(1)

$$Zn^{2+} + 2OH^- \rightarrow Zn(OH)_2 \downarrow \quad (2)$$

After hydrolysis treatment, the morphology of the resultant $Zn(OH)_2/SnO_2$/cellulose composite nanofibers was still smooth and round, and diameter remained basically unchanged, suggesting that the hydrolysis in mild base condition would not cause conceivable morphology and diameter changes (Fig. 2c).

Fig. 3 shows the SEM images of ZnO/SnO_2 composite nanofibers with different Zn:Sn molar ratio obtained at calcination temperature of 500, 700 and 900 °C. Different from the sheet-like nanoparticles obtained from the calcination of the $Zn(OAc)_2/SnO_2$/CA composite nanofibers, the ZnO/SnO_2 composite nanofibers were formed after calcination of $Zn(OH)_2/SnO_2$/cellulose composite nanofibers. This is due to that the fiber template cellulose component is a thermosetting polymer with a T_d at 260–295 °C. The ZnO/SnO_2 composite nanofibers were largely kept the fiber morphology after calcination at 500 °C and 700 °C (Fig. 3a, b, d, e, g, h), whereas the fiber structure was substantially destroyed after calcination at 900 °C (Fig. 3c, f, i). Pan et al. reported a similar phenomenon for the calcination of ZnO nanofibers [35]. It was also found that the mean fiber diameter decreased with the increasing of calcination temperature. For instance, the mean fiber diameter decreased from 47 ± 5 nm (Z_2S-5, Fig. 3d) to 36 ± 5 nm (Z_2S-7, Fig. 3e) as the calcination temperature increased from 500 to 700 °C.

TEM images (Fig. 4) of the ZnO/TiO_2 composite nanofibers showed that the ZnO/SnO_2 composite nanofibers were composed of grain-like nanoparticles whose size increased with increasing of the calcination temperature. Moreover, many disordered wormhole-like mesopores were found on the composite nanofibers, implying that some porous structures were destroyed during the calcination. This is due to the collapse of meso-structured walls and the aggregation of nanofibers [36]. Additionally, compared with the Z_2S-5, the pore size of Z_2S-7 became larger (highlighted by circles), indicating that the pore size increased with calcination temperature. The selected area electron diffraction (SAED) images suggested the polycrystalline nature of the mesoporous ZnO/SnO_2 composite nanofibers (Fig. 4, inset).

The typical XRD patterns of the mesoporous ZnO/SnO_2 composite nanofibers with Zn:Sn molar ratio of 2:1 calcined at different temperature for 5 h are shown in Fig. 5. From the XRD patterns, the mean crystallite sizes of ZnO and SnO_2 of the ZnO/SnO_2 composite nanofibers were calculated using the Scherrer formula and were listed in Table 1. Diffraction peaks of pure ZnO and SnO_2 nanofibers are perfectly indexed to the hexagonal wurtzite structure (JCPDS, #36-1451) for Z-5 (Fig. 5a) and a tetragonal rutile structure (JCPDS, #41-1445) for S-5 (Fig. 5b), suggesting high crystallinity of pure ZnO and SnO_2 nanofibers was obtained after calcination at 500 °C for 5 h. With calcination temperature increasing from 500 to 900 °C, the mean crystallite size of the ZnO and SnO_2 increased from 48.6 to 170.2 nm and 16.3 to 45.2 nm, respectively (Table 1). For all the mesoporous ZnO/SnO_2 composite nanofibers, the phase composition was the mixture of ZnO and SnO_2 when calcined at 500 °C for 5 h (Fig. 5c), but became mixture of ZnO, SnO_2 and Zn_2SnO_4 when calcined at 700 and 900 °C for 5 h (Fig. 5d and e). A solid reaction

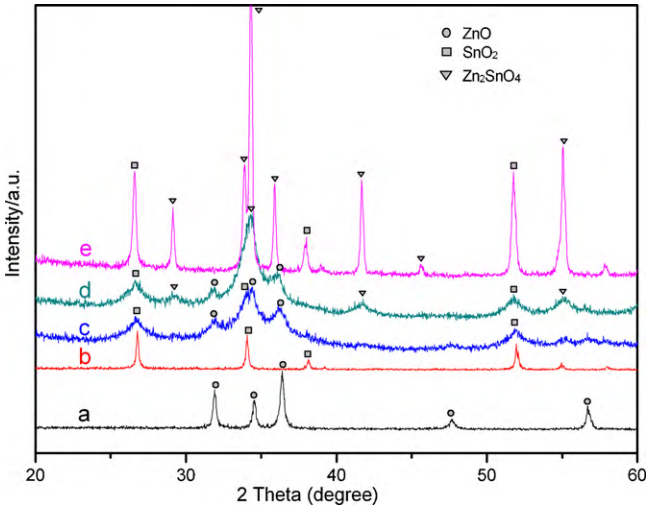

Fig. 5. XRD patterns of the mesoporous ZnO/SnO_2 composite nanofibers: (a) Z-5, (b) S-5, (c) Z_2S-5, (d) Z_2S-7, (e) Z_2S-9.

Table 1
The mean crystallite size of ZnO/SnO_2 composite nanofibers obtained at different calcination temperature.

Sample	Sn content (mol%)	Phase	Mean crystallite size (nm)		
			500 °C	700 °C	900 °C
Z	0	ZnO	48.6	82.3	170.2
Z_3S	25	ZnO	32.6	58.6	100.6
		SnO_2	2.0	A few	A few
		Zn_2SnO_4	–	36.2	78.2
Z_2S	33.3	ZnO	22	48.6	A few
		SnO_2	3.3	7.8	10.2
		Zn_2SnO_4	–	40.2	80.2
ZS	50	ZnO	28.5	A few	A few
		SnO_2	4.5	11.2	25.3
		Zn_2SnO_4	–	30.4	65.3
S	100	SnO_2	16.3	26.3	45.2

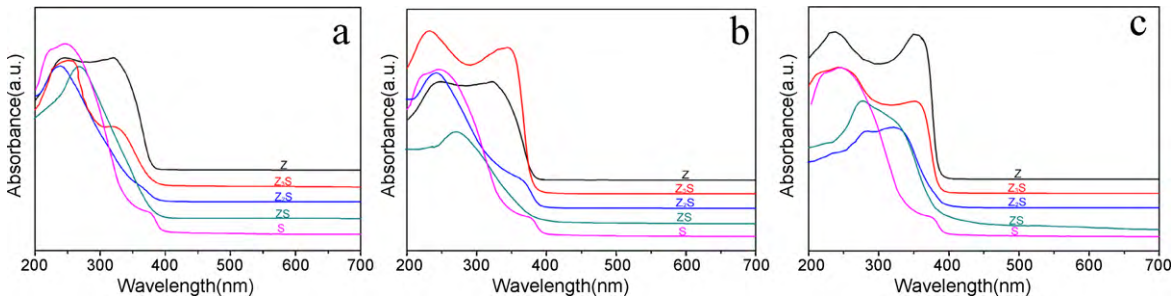

Fig. 6. UV–vis diffuse reflectance absorption spectra of the mesoporous ZnO/SnO_2 composite nanofibers calcined at different temperature for 5 h: (a) 500 °C, (b) 700 °C, (c) 900 °C.

between the ZnO and SnO_2 occurred to form an inverse spinel-type Zn_2SnO_4 phase (JCPDS, #74-2184) at 700 and 900 °C. The reaction between ZnO and SnO_2 to form Zn_2SnO_4 is expressed as following [37]:

$$2ZnO + SnO_2 \rightarrow Zn_2SnO_4 \quad (3)$$

The diffraction peaks are continuously getting sharper with increasing of the calcination temperature, suggesting that the crystallite size becomes larger at higher calcination temperature. This is in agreement with the results shown in TEM images (Fig. 4). Table 1 showed that the mean crystallite size of ZnO was always much larger than that of SnO_2 under the same calcination temperature. This is because that ZnO sinters more easily, and therefore it tends to form larger grain size [38]. Additionally, the average crystallite size of SnO_2 and ZnO in the SnO_2/ZnO composite nanofibers is slightly smaller than that of pure SnO_2 and pure ZnO nanofibers (Table 1). It has been reported that the addition of SnO_2 into ZnO causes a reduction in the mean crystallite size of ZnO and SnO_2 [39,40].

The DRS of mesoporous ZnO/SnO_2 composite nanofibers are shown in Fig. 6. For comparison, the DRS of pure ZnO and SnO_2 nanofibers are also presented. The wavelength of absorption edge is determined by extrapolating the horizontal and sharply rising portions of the curve and defining the edge as the wavelength of the intersection [41]. The absorption edges and the band gap energies (E_g) calculated on the basis of the corresponding absorption edges are shown in Table 2. The band gap absorption edge of ZnO calcined at 500, 700 and 900 °C are determined to be 386.5, 388.2 and 390.1 nm, corresponding to the E_g of 3.21, 3.19 and 3.18 eV, respectively. They are in reasonable agreement with the values of 3.2 eV reported in the literature [42]. The band gap absorption edge of SnO_2 calcined at 500, 700 and 900 °C are determined to be 401.0, 402.0 and 402.3 nm, corresponding to the E_g of 3.09, 3.08 and 3.08 eV, indicating that the E_g of the SnO_2 has little relation with the calcination temperature. However, this value is much less than the reported value of 3.8 eV [43]. It was reported that SnO_2 is a n-type semiconductor oxide with not only the direct E_g of 3.5–3.9 eV, but also an indirect E_g of ~2.6 eV, so the band gap value of SnO_2 nanofibers indicates an indirect transition as reported by Seftel [44] and Wang et al. [45]. Table 2 shows that the E_g of ZnO/SnO_2 composite nanofibers fall in between that of neat ZnO and SnO_2. This is due to that their E_g are the contribution of the corresponding ZnO, SnO_2 and/or Zn_2SnO_4 crystallite phases in the composite nanofibers. For the ZnO/SnO_2 composite nanofibers with a fixed Zn:Sn, their E_g slightly decreased with the calcination temperature (Table 2).

Zhang et al. [46] realized that the E_g of materials are related to their photocatalytic activity. The larger the E_g of a material is, the greater the redox potential for the photogenerated electron–hole

Table 2
The composition, calcination temperature, absorption edge and band gap energy of ZnO/SnO_2 composite nanofibers.

Sample	Sn content (mol%)	Absorption edge (nm)			Band gap energy (eV)		
		500 °C	700 °C	900 °C	500 °C	700 °C	900 °C
Z	0	386.5	388.2	390.1	3.21	3.19	3.18
Z_3S	25	389.1	391.3	393.7	3.19	3.17	3.15
Z_2S	33.3	390.3	393.2	394.5	3.18	3.15	3.14
ZS	50	395.0	396.3	396.1	3.14	3.13	3.13
S	100	401.0	402.1	402.3	3.09	3.08	3.08

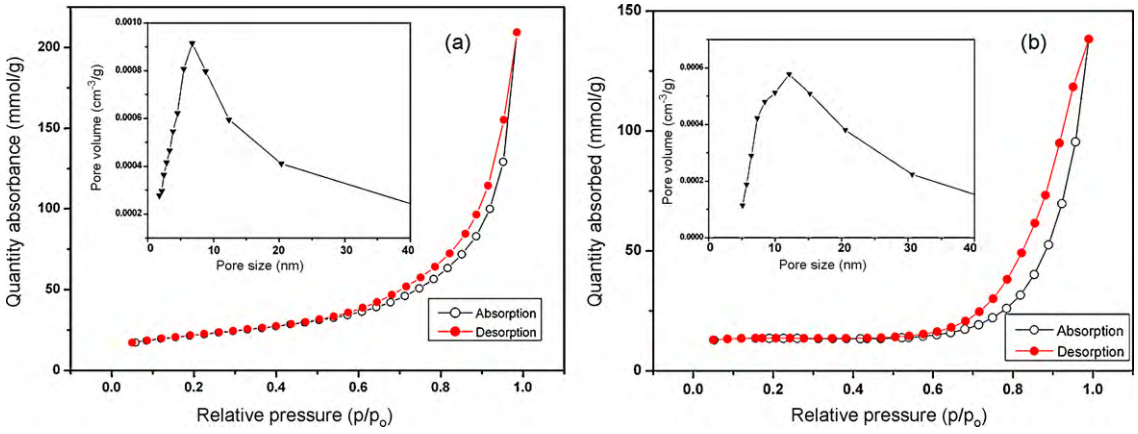

Fig. 7. Nitrogen absorption–desorption isotherms of mesoporous ZnO/SnO_2 composite nanofibers, inset is pore size distribution image of corresponding composite nanofibers: (a) Z_2S-5 and (b) Z_2S-7.

is. So the ZnO/SnO_2 composite nanofibers calcined at 500 °C would show higher photocatalytic activity than those calcined at 700 and 900 °C, as will be discussed in the later section.

To further understand the pore structure of mesoporous ZnO/SnO_2 composite nanofibers, their N_2 adsorption and desorption isotherms were measured. The typical N_2 adsorption–desorption isotherms and pore size distributions of Z_2S-5 and Z_2S-7 are shown in Fig. 7. They exhibited a type IV isotherms with type H_3 hysteresis when the relative pressure P/P_o is in the range of 0.6–1.0 according to the IUPAC nomenclature. This is a characteristic process between adsorption into and desorption from the mesopores [47]. The insets in Fig. 7 are the corresponding pore size distribution (PSD) curves, which were derived by the Barret–Joyner–Halenda (BJH) method. They revealed a pore size distribution centered at about 6.7 nm (Fig. 7a) and 13.6 nm (Fig. 7b) for the Z_2S-5 and Z_2S-7 nanofibers, respectively. In addition, the Brunauer–Emmett–Teller (BET) analysis showed that the surface areas of the Z_2S-5 and Z_2S-7 were 78.2 and 39.8 $m^2\,g^{-1}$, respectively, indicating that the surface areas decreased with the increasing of the calcination temperature. This is because that the grain size increased with increasing of the calcination temperature, as shown in the TEM images (Fig. 4). The pore sizes and surface areas of ZnO/SnO_2 composite nanofibers are summarized in Table 3. For composite nanofibers calcined at a same temperature, it is obviously noted that the molar ratio of Zn:Sn had little effect on the pore size and surface areas. The fully thermal decomposition of cellulose fiber template, which accounts for nearly 90 wt.% of the precursor composite fiber, is the main reason for the formation of mesopores in the metal oxide nanofibers. Therefore, the different molar ratio of Zn:Sn showed little effect on the porosity. However, the calcination temperature affects the porosity because the crystallite growth greatly depends on the temperature (Table 1, Fig. 5).

RhB has often been used as a model dye molecule for photocatalytic degradation by a transition metal oxide [48,49]. The photocatalytic activity of mesoporous ZnO/SnO_2 composite nanofibers was evaluated by the photocatalytic decomposition of RhB dye under the irradiation of UV light. Fig. 8 shows the absorbance spectra of RhB aqueous solutions in the presence of Z_2S-5 after UV irradiation. It can be seen that the maximum absorbance at 554 nm disappears completely after irradiation for 60 min. Moreover, the maximum absorbance peak showed blue shift from 554 to 521 nm after irradiation. This should result from the formation of a series of N-de-ethylated intermediates in a stepwise manner. Similar phenomena were also observed during the photodegradation of sulforhodamine B [50] and RhB [51] under visible light irradiation.

The photocatalytic degradation rates of RhB with the mesoporous ZnO/SnO_2 composite nanofibers are shown in Fig. 9. In addition to photocatalytic experiments in the presence of Z_2S-5, two control experiments were performed in the absence of Z_2S-5 with UV irradiation or in the presence of Z_2S-5 without UV irradiation (Fig. 9a). RhB was hardly degraded under the control experimental conditions. However, in the presence of UV irradiation and Z_2S-5, RhB was photo-degraded rapidly (Fig. 9a). From the almost linear relationship between C/C_o and t, a first-order degradation mechanism was suggested for all the samples in the degradation period tested in this research. The degradation rate constants of RhB by ZnO/SnO_2 composite nanofibers were listed in Table 4. The photocatalytic activity follows the order of Z_2S-5 > Z_3S-5 > ZS-5 > Z-5 > S-5. The ZnO/SnO_2 composite nanofibers showed higher photocatalytic activity than pure ZnO and SnO_2 nanofibers. Moreover, the Z_2S-5 showed the strongest photocatalytic activ-

Table 3
The composition, calcination temperature, pore size and surface areas of ZnO/SnO_2 composite nanofibers.

Sample	Sn content (mol%)	Pore size (nm)		Surface areas ($m^2\,g^{-1}$)	
		500 °C	700 °C	500 °C	700 °C
Z_3S	25	6.5	13.6	76.5	38.2
Z_2S	33.3	6.7	13.6	78.2	39.8
ZS	50	6.8	13.5	75.2	37.6

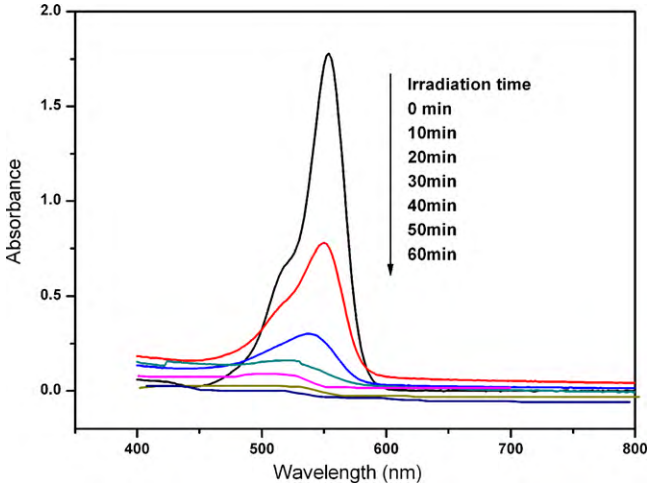

Fig. 8. The absorbance spectra changes of Rhodamine B in an aqueous solution in the presence of Z_2S-5 after different irradiation times.

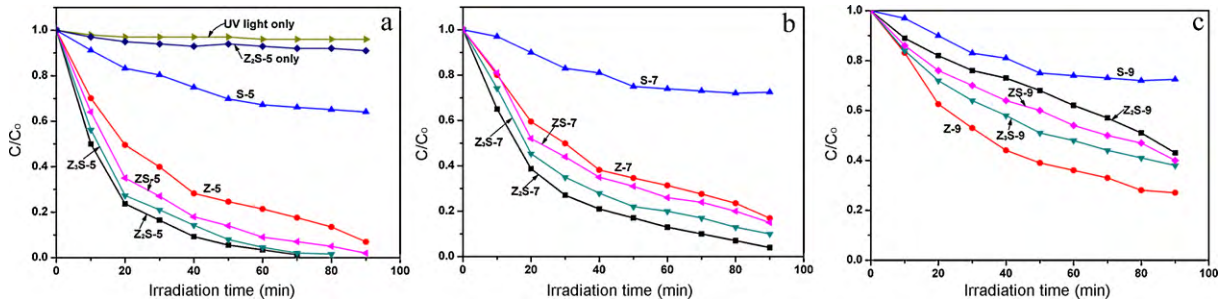

Fig. 9. Photocatalytic degradation of Rhodamine B aqueous solutions by ZnO/SnO_2composite nanofibers calcined at (a) 500 °C, (b) 700 °C, (c) 900 °C.

Table 4
Degradation rate constants of RhB using ZnO/SnO_2 composite nanofibers photocatalysts.

Sample	Rate constant, k (min^{-1})	Sample	Rate constant, k (min^{-1})	Sample	Rate constant, k (min^{-1})
Z-5	0.024	Z-7	0.020	Z-9	0.018
Z_3S-5	0.046	Z_3S-7	0.027	Z_3S-9	0.012
Z_2S-5	0.051	Z_2S-7	0.031	Z_2S-9	0.008
ZS-5	0.035	ZS-7	0.024	ZS-9	0.010
S-5	0.007	S-7	0.002	S-9	0.001

ity than the other samples. This is attributed to its high surface areas, high efficiency in the light utilization and high efficient separation of photogenerated electron/hole pairs (showed in the following section). It can be seen that the photocatalytic activity was decreased with increasing of the calcination temperature for composite nanofibers with a fixed Zn:Sn ratio. This is because the Zn_2SnO_4 generated at 700 and 900 °C showed lower photocatalytic activity than ZnO [45], and the surface areas decreased with increasing of the calcination temperature.

Many researches have proved that an optimal composition ratio is necessary to maximize the lifetime of photogenerated electrons [44,51]. This is also the case for the mesoporous ZnO/SnO_2 composite nanofibers. When the content of SnO_2 was as low as 25 mol%, the effect of photogenerated electron trapped by SnO_2 was not obvious because of the insufficiency of SnO_2. The photocatalytic activity was thus not the highest. When the content of SnO_2 was as high as 50 mol%, some ZnO active sites would be surrounded by SnO_2. This would hinder the contact between ZnO and oxygen containing species, resulting in the reduction of the photocatalytic activity. In this study, the optimal ZnO/SnO_2 composition was found to be Zn:Sn = 2:1. And the Z_2S-5 showed the highest photocatalytic among Z_2S-5, Z_3S-5 and ZS-5.

Fig. 10 shows the mechanism of the charge separation and photocatalytic reaction for the mesoporous Z_2S-5 photocatalysts. As illustrated in the scheme, when the Z_2S-5 photocatalysts are irradiated by UV light with a photon energy higher or equal to the band gaps of ZnO and SnO_2, electrons (e^-) in the valence band (VB) are excited to the conduction band (CB) with simultaneous generation of the same amount of holes (h^+) in the VB (Eq. (4)). Because the CB of SnO_2 is lower than that of ZnO, upon light-activation the electrons transfer from the CB of ZnO to that of SnO_2, and SnO_2 acts as a sink for the photogenerated electrons. Conversely, the holes transfer from the VB of SnO_2 to that of ZnO (Eq. (5)). The photogenerated electrons and holes in the Z_2S-5 photocatalysts could inject into a reaction medium and participate in chemical reactions [46,52].

$$ZnO/SnO_2 \xrightarrow{h\nu} ZnO(e_{cb}^- \cdots h_{vb}^+)/SnO_2(e_{cb}^- \cdots h_{vb}^+) \quad (4)$$

$$ZnO(e_{cb}^- \cdots h_{vb}^+)/SnO_2(e_{cb}^- \cdots h_{vb}^+) \longrightarrow ZnO \cdot h_{vb}^+ / SnO_2 \cdot e_{cb}^- \quad (5)$$

The electronic acceptors like adsorbed O_2 can easily trap the photogenerated electron (e^-) to produce a superoxide anion radical ($^\bullet O_2^-$), and hydroxyl radicals ($^\bullet$OH) are formed by the reaction of the photoinduced hole (h^+) with adsorbed H_2O. The formed $^\bullet O_2^-$ were reacted with e^- and H^+ to produce H_2O_2, which would provide hydroxyl radical ($^\bullet$OH) by acting as a direct electron acceptor by reaction with e^- and $^\bullet O_2^-$. The hydroxyl radical ($^\bullet$OH) is an extremely strong oxidant for the partial or complete mineralization of organic chemicals [53]. The following photocatalytic reactions possibly occur:

$$e_{cb}^- + O_2 \rightarrow {}^\bullet O_2^- \quad (6)$$

$$h_{vb}^+ + H_2O \rightarrow H^+ + {}^\bullet HO \quad (7)$$

$$^\bullet O_2^- + H^+ \rightarrow {}^\bullet HO_2 \quad (8)$$

$$^\bullet HO_2 + e_{cb}^- + H^+ \rightarrow H_2O_2 \quad (9)$$

$$H_2O_2 + e_{cb}^- \rightarrow {}^\bullet OH + OH^- \quad (10)$$

$$H_2O_2 + {}^\bullet O_2^- \rightarrow {}^\bullet OH + OH^- + O_2 \quad (11)$$

$$^\bullet OH + RhB \rightarrow CO_2 + H_2O \quad (12)$$

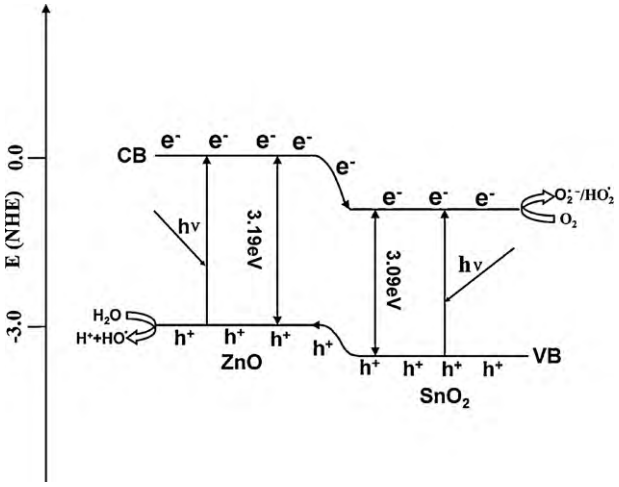

Fig. 10. The schematic illustration of the electron transfer and the energy level diagram indicating the band positions of the ZnO and SnO_2 in the photocatalytic system.

Therefore, efficient charge separation increases the lifetime of the charge carriers and reduces the recombination of the hole–electron pairs in the composite nanofibers, thus increases the quantum efficiency [52]. This results in the strongest photocatalytic efficiency for Z_2S-5 nanofibers among the ZnO/SnO_2 composite nanofibers prepared in this research.

4. Conclusions

Mesoporous ZnO/SnO_2 composite nanofibers with high photocatalytic activity were successfully synthesized through electrospinning. Their crystal phase compositions, mean crystallite sizes, band gap energies, as well as photocatalytic efficiency, were studied in relation to the molar ratio of Zn:Sn and calcination temperatures. TEM images showed that the mesoporous ZnO/SnO_2 composite nanofibers were composed of grain-like nanoparticles. The photocatalytic activity of the mesoporous ZnO/SnO_2 reached the maximum when the molar ratio of Zn:Sn was 2:1 and the calcination temperature was about 500 °C for 5 h. The enhancement of the photocatalytic activity is attributed to the high BET surface areas, high efficiency in the light utilization and high efficient separation of photogenerated electron/hole pairs. The electrospinning method reported in this manuscript can be extended to the preparation of other mesoporous semiconductor composite nanofibers for the treatment of wastewater.

Acknowledgements

This work is supported by the National Natural Science Foundation of China (no. 50973019, 50843030), the National Basic Research Program of China (2010CB732203), the Key Project of Natural Science Foundation of Fujian Province (Grant no. E0620001), and the Initiative Fund for the Returned Overseas Chinese Scholar administered by the State Education Ministry.

References

[1] D. Ravelli, D. Dondi, M. Fagnoni, A. Albini, Chem. Soc. Rev. 38 (2009) 1999.
[2] S. Malato, P. Fernandez-Ibanez, M.I. Maldonado, J. Blanco, W. Gernjak, Catal. Today 147 (2009) 1.
[3] J.H. Zhang, X. Xiao, J.M. Nan, J. Hazard. Mater. 176 (2010) 617.
[4] S. Sreekantan, L.C. Wei, J. Alloys Compd. 490 (2010) 436.
[5] K. Rajeshwar, M.E. Osugi, W. Chanmanee, C.R. Chenthamarakshan, M.V.B. Zanoni, P. Kajitvichyanukul, R. Krishnan-Ayer, J. Photochem. Photobiol. C 9 (2008) 171.
[6] A. Rachel, M. Subrahmanyam, P. Boule, Appl. Catal. B: Environ. 37 (2002) 301.
[7] J. Yang, J. Zhang, L.W. Zhu, S.Y. Chen, Y.M. Zhang, Y. Tang, Y.L. Zhu, Y.W. Li, J. Hazard. Mater. 137 (2006) 952.
[8] T.S. He, Z.F. Zhou, W.B. Xu, F.M. Ren, H.H. Ma, J. Wang, Polymer 50 (2009) 3031.
[9] M. Nikazar, K. Gholivand, K. Mahanpoor, Desalination 219 (2008) 293.
[10] T.S. He, H.H. Ma, Z.F. Zhou, W.B. Xu, F.M. Ren, Z.F. Shi, J. Wang, Polym. Degrad. Stab. 94 (2009) 2251.
[11] M.A. Behnajady, N. Modirshahla, N. Daneshvar, M. Rabbani, J. Hazard. Mater. 140 (2007) 257.
[12] M.A. Behnajady, S.G. Moghaddam, N. Modirshahla, M. Shokri, Desalination 249 (2009) 1371.
[13] S.H. Lee, Y. Song, I.D. Hosein, C.M. Liddell, J. Mater. Chem. 19 (2009) 350.
[14] Z.Y. Liu, D.D.L. Sun, P. Guo, J.O. Leckie, Nano Lett. 7 (2007) 1081.
[15] S.H. Zhan, D.R. Chen, X.L. Jiao, C.H. Tao, J. Phys. Chem. B 110 (2006) 11199.
[16] A. Greiner, J.H. Wendorff (Eds.), Angew. Chem. Int. Ed. 46 (2007) 5670.
[17] Y.P. Fang, Q. Pang, X.G. Wen, B.N. Wang, S.H. Yang, Small 2 (2006) 612.
[18] J. Li, E.H. Liu, W. Li, X.Y. Meng, S.T. Tan, J. Alloys Compd. 478 (2009) 371.
[19] D. Li, Y.N. Xia, Adv. Mater. 16 (2004) 1151.
[20] J.G. Zhao, C.W. Jia, H.G. Duan, H. Li, E.Q. Xie, J. Alloys Compd. 461 (2008) 447.
[21] H.Q. Liu, J.X. Yang, J.H. Liang, Y.X. Huang, C.Y. Tang, J. Am. Ceram. Soc. 91 (2008) 1287.
[22] H.Y. Guan, C.L. Shao, S.B. Wen, B. Chen, J. Gong, X.H. Yang, Inorg. Chem. Commun. 6 (2003) 1302.
[23] Z.F. Zhou, Y. Feng, W.B. Xu, F.M. Ren, H.H. Ma, J. Appl. Polym. Sci. 113 (2009) 1264.
[24] C.H. Wang, C.L. Shao, L.J. Wang, L. Zhang, X.H. Li, Y.C. Liu, J. Colloid Interface Sci. 333 (2009) 242.
[25] R.L. Liu, H.Y. Ye, X.P. Xiong, H.Q. Liu, Mater. Chem. Phys. 121 (2010) 432.
[26] R. Zhang, H. Wu, D.D. Lin, W. Pan, J. Am. Ceram. Soc. 92 (2009) 2463.
[27] M.A. Kanjwal, N.A.M. Barakat, F.A. Sheikh, H.Y. Kim, J. Mater. Sci. 45 (2010) 1272.
[28] M. Jin, X. Zhang, A.V. Emeline, Z. Liu, D.A. Tryk, T. Murakami, A. Fujishima, Chem. Commun. 43 (2006) 4483.
[29] S.K. Kansal, M. Singh, D. Sud, J. Hazard. Mater. 141 (2007) 581.
[30] J. Yang, D. Li, X. Wang, X.J. Yang, L.D. Lu, J. Solid State Chem. 165 (2002) 193.
[31] Y. Zhang, J.P. Li, G.M. An, X.L. He, Sens. Actuat. B: Chem. 144 (2010) 43.
[32] X.F. Song, L. Liu, Sens. Actuat. A: Phys. 154 (2009) 175.
[33] J.A. Park, J. Moon, S.J. Lee, S.H. Kim, H.Y. Chu, T. Zyung, Sens. Actuat. B: Chem. 145 (2010) 592.
[34] H.Q. Liu, Y.L. Hsieh, J. Polym. Sci. B: Polym. Phys. 40 (2002) 2119.
[35] H. Wu, W. Pan, J. Am. Ceram. Soc. 89 (2006) 699.
[36] X.F. Song, W.Z. Wang, Y.B. Liu, W. Wang, L. Li, Nanotechnology 20 (2009) 75501.
[37] T. Hashemi, H.M. Al-Allak, J. Illingsworth, A.W. Brinkman, J. Woods, J. Mater. Sci. Lett. 9 (1990) 776.
[38] J.H. Yu, G.M. Choi, Sens. Actuat. B: Chem. 61 (1999) 59.
[39] C. Wang, X. Wang, B.Q. Xu, J. Zhao, B. Mai, P. Peng, G. Sheng, J.M. Fu, J. Photochem. Photobiol. A 168 (2004) 47.
[40] A. Recnik, N. Daneu, T. Walther, W. Mader, J. Am. Ceram. Soc. 84 (2001) 2657.
[41] P.L. Provenzano, G.R. Jindal, J.R. Sweet, W.B. White, J. Lumin. 92 (2001) 297.
[42] C. Wang, B.Q. Xu, X.M. Wang, J.C. Zhao, J. Solid State Chem. 178 (2005) 3500.
[43] A. Hagfeldt, M. Gratzel, Chem. Rev. 95 (1995) 49.
[44] E.M. Seftel, E. Popovici, M. Mertens, E.A. Stefaniak, R. Van Grieken, P. Cool, E.F. Vansant, Appl. Catal. B: Environ. 84 (2008) 699.
[45] C. Wang, J.C. Zhao, X.M. Wang, B.X. Mai, G.Y. Sheng, P. Peng, J.M. Fu, Appl. Catal. B: Environ. 39 (2002) 269.
[46] M.L. Zhang, T. An, X. Hu, C. Wang, G. Sheng, J.M. Fu, Appl. Catal. A: Gen. 260 (2004) 215.
[47] K.S.W. Sing, D.H. Everett, R.A.W. Haul, L. Moscou, R.A. Pierotti, J. Rouquerol, T. Siemieniewska, Pure Appl. Chem. 57 (1985) 603.
[48] G. Liu, G.S. Li, X.Q. Qiu, L.P. Li, J. Alloys Compd. 481 (2009) 492.
[49] Z.J. Zhang, W.Z. Wang, M. Shang, W.Z. Yin, J. Hazard. Mater. 177 (2010) 1013.
[50] C. Chen, W. Zhao, J. Li, J. Zhao, H. Hidaka, N. Serpone, Environ. Sci. Technol. 36 (2002) 3604.
[51] Z. He, C. Sun, S. Yang, Y. Ding, H. He, Z. Wang, J. Hazard. Mater. 162 (2009) 1477.
[52] K. Tennakone, J. Bandara, Appl. Catal. A: Gen. 208 (2001) 335.
[53] F. Kiriakidou, D.I. Kondarides, X.E. Verykios, Catal. Today 54 (1999) 119.